Excitation functions of ^{3}He-particle induced nuclear reactions on ^{103}Rh: Experimental and theoretical investigations

B. M. Ali[a], M. Al-Abyad[a], S. Kandil[a], A. H. M. Solieman[a], F. Ditrói[b]

[a] *Physics department (Cyclotron Facility), Nuclear Research Centre, Atomic Energy Authority, Cairo 13759, Egypt*

[b] *Institute for Nuclear Research (ATOMKI), Hungarian Academy of Sciences, Debrecen H4026, Hungary*

Abstract

Excitation functions for the ^{3}He-induced reactions on ^{103}Rh as alternative pathway for the production of the medically used ^{103}Pd were studied by the stacked foil technique. Excitation functions of the ^{103}Rh(^{3}α, x) ^{103}Pd, ^{103,104,104m,105}Ag and ^{100,101,101m,102,102m}Rh reactions were determined up to 27 MeV by detecting only the characteristic γ-rays obtained from the decay of residual nuclei. The experimental results were compared with the theoretical ones obtained from the EMPIRE-3.2 code and the TENDL nuclear data library. From the measured cross-section data integral production yields were calculated.

Keywords: ^{3}He induced nuclear reactions; ^{100,101,102}Rh, ^{103}Pd, ^{103}Rh, ^{103,104,105}Ag radioisotopes, Excitation function; Stacked-foil technique; Integral yield

Introduction

Excitation functions of charged particles induced nuclear reactions on ^{103}Rh for protons, deuteron and alpha particles have already been studied. The measurements and nuclear model calculations have reported for the proton-induced reactions on ^{103}Rh target covering the energy range up to 40 MeV [1-4]. The study of deuteron and alpha activation reactions has been measured up to 50 MeV [5, 6]. The excitation function for the ^{3}He-particle has no previous experiment.

Among all radionuclides produced the palladium-103 is the most important, having a half-life of 16.99 d and decaying 100% by the electron capture (EC) process to ^{103m}Rh ($T_{1/2}$ = 56.1 min). It is ideally suited for interstitial brachytherapy, particularly for the treatment of prostate cancer. In addition to the production of ^{103}Pd by charged particles activation, it is also formed by indirect route through the decay of ^{103}Ag.

Due to the increasing need of this widely used therapeutic radionuclide ^{103}Pd, a search for alternative routes of its production using other charged particle beams appears to be important. The present work will investigate the possibility of its production in nuclear reactions induced by accelerated ^{3}He ions on rhodium. For other radionuclides a due consideration will also be given.

Experimental

Cross-sections were measured by the activation method using the stacked-foil technique at MGC-20E cyclotron of the Institute for Nuclear Research (ATOMKI), Debrecen, Hungary. The experimental set-up and data processing were similar to that described in our earlier publications [7,8]. High purity natural rhodium foils (>99.98 % supplied by Goodfellow, England) with a thickness of 12 μm were assembled together with natural titanium foils with a thickness of 12 μm in one stack. The stack consisted of 14 high purity natural Rh foils and 3 high purity natural Ti monitor foils. It was irradiated in a Faraday-cup like target holder with collimator and secondary electron suppresser. Irradiation took place for one hour using 27 MeV primary incident ^{3}He-particle beam with a constant current of 100 nA. The energy and flux of the extracted beam were derived from the accelerator setting parameters and the charge integrated on the Faraday-cup. The monitors were used as projectile energy degrader, recoil catchers and for exact determination of the beam intensity and energy by re-measuring the excitation function of the ^{nat}Ti(^{3}He,x)^{48}V reaction over the entire energy domain. For energy degradation along the stack, the stopping power of ^{3}He-particles was calculated using the SRIM-2013 code [9]. The uncertainty of energy increases along the stack due to cumulative effects, it reaches its maximum of ±1.4 MeV at the last foil.

The activity of the produced radionuclides was measured with standard high resolution γ-ray spectrometer consisting of HPGe detectors coupled to multi-channel analyzers. The spectra were measured at large distances to avoid coincidence losses. Detector efficiencies for different measuring distances were carefully determined using different standard sources. There was no chemical separation after the irradiation. Spectra analysis were done using γ-analysis program FGM [10]. Measurements of the induced activity started shortly after EOB (End of Bombardment) and repeated four times after different cooling times.

The cross-sections were calculated from the well-known activation formula taking into account the measured activity, the particle flux and the number of target nuclei. The decay data and Q-values were taken from NuDat 2.6 data base [11]. Individual and cumulative processes were taken into account. The beam energy and intensity parameters were adapted by comparing the excitation function of the monitor reaction ^{nat}Ti(^{3}He,x)^{48}V with the recommended values of the IAEA-TECDOC 1211 [12, 22] (Fig. 1).

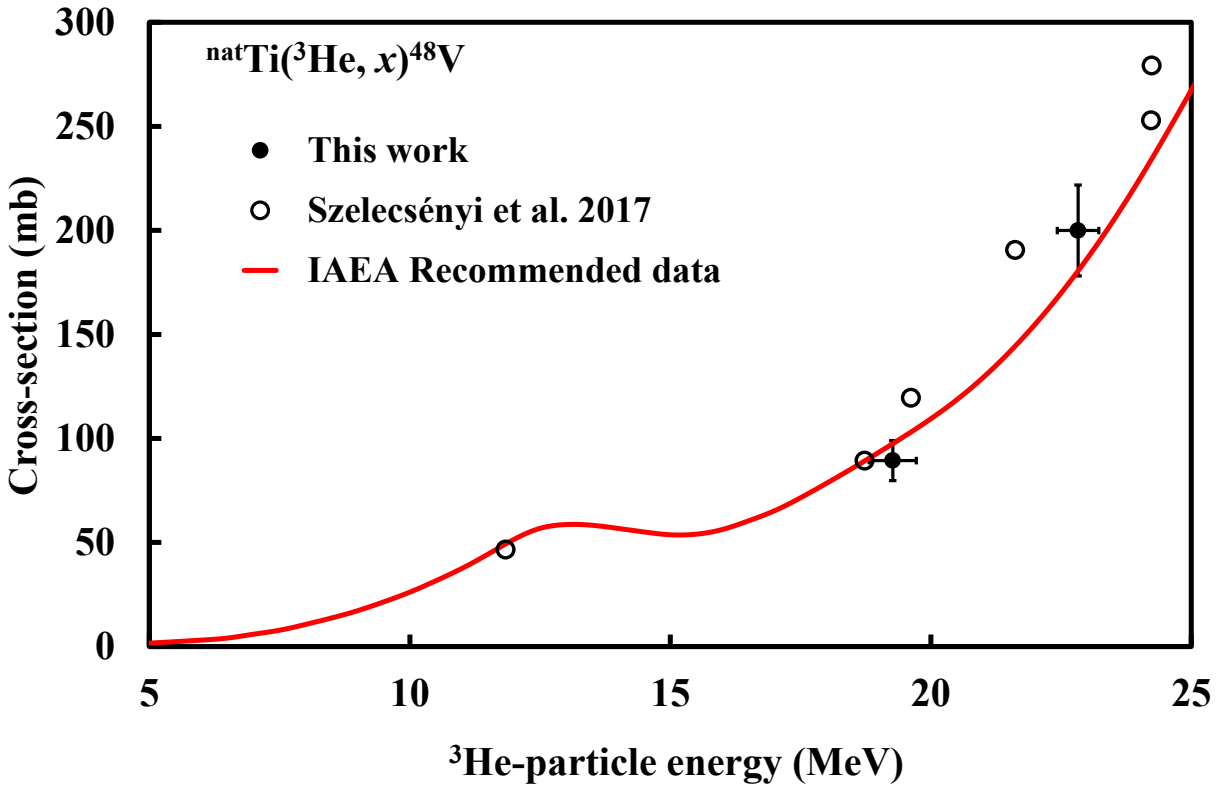

Fig 1: Recommended excitation function of the monitor reaction ^{nat}Ti(^{3}He,x)^{48}V compared to that obtained from the monitor foils.

The uncertainty on each cross-section point was estimated in the standard way [13] by taking the square root of the sum in quadrature of all individual contributions. The following individual uncertainties are included in the error calculations: incident particle intensity (7 %), determination of the peak areas including statistical errors (3 %), decay data (3 %), the number of target nuclei including non-uniformity (5 %) and detector efficiency (7 %). The total uncertainty of the cross-sections was evaluated to be approximately 12 % and, in some cases it was higher.

Results and Discussion

In the present work, the contributing reactions of each product and their Q-values are given in Table 1, the numerical values of the measured cross sections of the ^{3}He-induced reactions are presented in Tables 2-4 and the excitation functions are depicted in the Figs. 2-11. Having surveyed the literature on the excitation functions of the studied reactions we found no earlier publication. The cross-sections for ^{103}Rh(^{3}He,x) reactions were measured by detecting characteristic γ-rays obtained from the decay of residual nuclei. In the present measurement, we have considered only those γ-rays that gave appreciable activities for meaningful studies. The experimental results were

compared with the theoretical model calculations obtained from the EMPIRE-3.2 [24, 25] code and the TENDL [23] nuclear data library.

Excitation function for the radio-silver production

Formation of ^{105}Ag

The residual nucleus ^{105}Ag produced through ^{103}Rh(^{3}He, n) reaction exists in two states. The meta-stable state ^{105m}Ag ($T_{1/2}$ = 7.23 min) decays completely through isomeric transition (IT, 100%) to the ground state ^{105g}Ag ($T_{1/2}$ = 41.29 d). In this case the cumulative cross-section was measured by allowing for complete decay of the metastable state to the ground state.

The measured excitation function of m+g states reaches its maximum value around 23.6 MeV of about 4.3 mb (Fig. 2). The experimental data obtained were compared with the results of both EMPIRE and TENDL calculations. EMPIRE calculation relates the cumulative cross section to the m and g states with experimentally similar trend of excitation functions but have their maximum at 19.0 MeV, with 62% and 38% weights respectively. TENDL calculation overestimates the values of excitation function all through the studied energy range, and fails to reproduce the experimental shape of the excitation function and gives a higher results up to 1400 mb (it could be wrong). While TALYS results are in the same order of the experimental data and EMPIRE results as well.

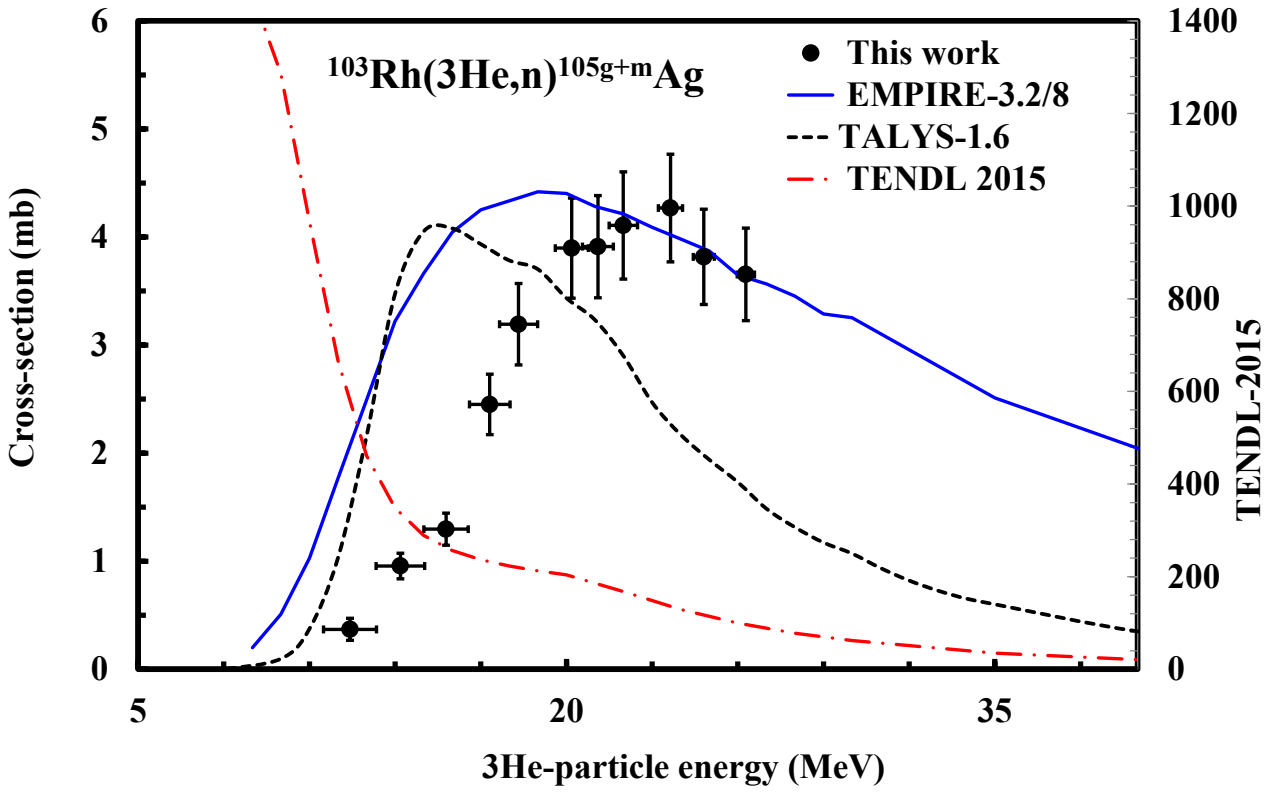

Fig 2: Excitation function of the $^{103}Rh(^{3}He,n)^{105g+m}Ag$ reaction.

Formation of ^{104}Ag

^{104}Ag radionuclide has two isomeric states, a relatively long-lived ground state ^{104g}Ag ($T_{1/2}$ = 69.2 min) and a shorter-lived meta-stable state ^{104m}Ag ($T_{1/2}$ = 33.5 min). ^{104m}Ag makes a very low IT (0.07%) contribution to its ground state ^{104g}Ag, but makes a large EC + β^+ (99.93%) decay to the stable isotope ^{104}Pd followed by the emission of intense γ-lines of 555.8 keV (90%), 785.7 keV (1.9%) and 1238.8 keV (3.9%). The strong and intense 555.8 keV (90%) γ-line is also the characteristic γ-line of the ground state ^{104g}Ag radionuclide. As the half-life of ^{104m}Ag ($T_{1/2}$ = 33.5 min) isomer is comparable to the half-life of its ground state ^{104g}Ag ($T_{1/2}$ = 69.2 min), therefore, it was difficult to separate the contribution of ^{104m}Ag from the common γ-line of 555.8 keV by using decay curve analysis (i.e., applying a suitable cooling time). We therefore separated the contribution of ^{104m}Ag activity using the basic activity distribution law [14, 15] utilizing the fact that the activity for a particular radionuclide should be same to its different characteristics γ-lines. The nuclide, ^{104m}Ag was therefore identified using the 555.8 keV γ-line. There is no possible precursor contribution to ^{104m}Ag, and hence, the measured cross-section of $^{103}Rh(^{3}He, 2n)^{104m}Ag$ process is treated as independent cross-section (Fig. 3).

The ^{104m}Ag excitation function has defined peak around about 19 MeV with a maximum value of about 145 mb. Theoretical calculations of EMPIRE and TENDL fail to describe the experimental excitation function, producing a high energy long tailed peak with much less maximum value at energies of 15.5 MeV and 16 MeV respectively.

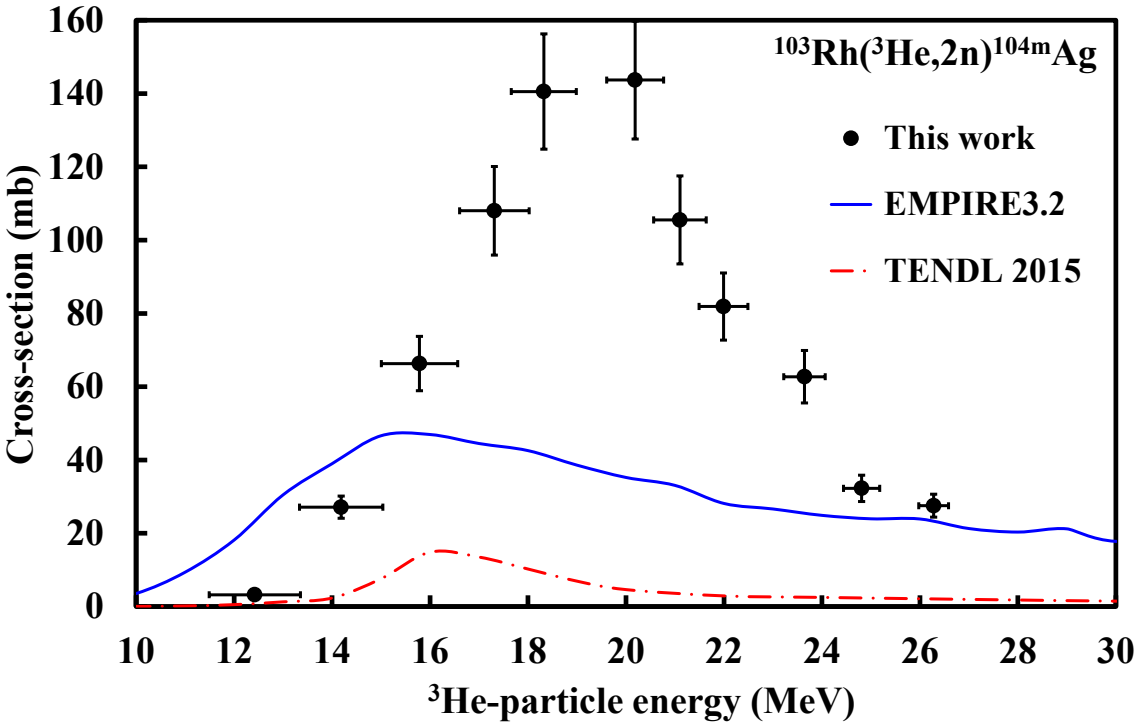

Fig 3: Excitation function of the ^{103}Rh(^{3}He,2n)^{104m}Ag reaction.

The ^{104g}Ag radionuclide was populated followed by the neutron emission, depicting the direct reaction process. No precursor decay was identified in the formation of ^{104g}Ag radionuclide. ^{104g}Ag was identified by its strong and independent γ-lines of 767.6 keV (65.7%) and 941.6 keV (25%), and a consistent result was found between them. Due to the negligible IT (0.07%) decay of the ^{104m}Ag isomer to its ground state competitor ^{104g}Ag, which is much smaller than the experimental error (11-25%), the production cross-sections of ^{104g}Ag are considered to be independent. Hence, the measured excitation function will be assigned to ^{103}Rh(^{3}He, 2n)^{104g}Ag process, in favor of cumulative cross section (Fig. 4).

The excitation function of ^{103}Rh(^{3}He, 2n)^{104g}Ag shows a peak at 17.5 MeV with a maximum cross-section of about 157 mb (Fig. 4). Its experimental threshold around 12.4 MeV and it has a low cross section values characterizing the (^{3}He, 2n) reactions in general [16, 17]. The measured production cross section of ^{104g}Ag is very close to that of the meta-state.

EMPIRE calculation has nearly same trend of ^{104g}Ag experimental excitation function, but its magnitude is about 2.5 times higher than the experimental one. On the other hand, the TENDL data are significantly lower in magnitude and show similar trend as the experimental (Fig. 4). TENDL data could successfully reproduce the experimental isomeric ratio, while EMPIRE gives about two orders of magnitude more weight for the ground state.

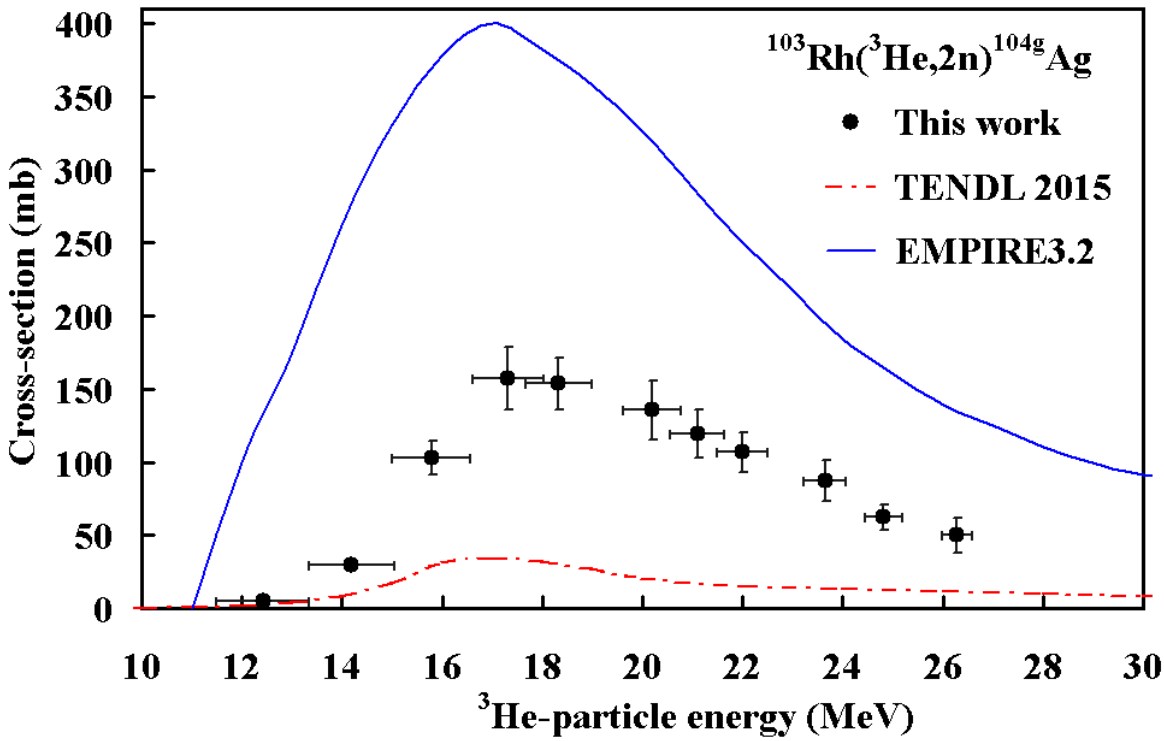

Fig 4: Excitation function of the ^{103}Rh(^{3}He,2n)^{104g}Ag reaction.

Formation of ^{103}Ag

The radionuclide ^{103}Ag has two isomeric states, ^{103g}Ag ($T_{1/2}$ = 65.7 min) and a very short-lived meta-stable state ^{103m}Ag ($T_{1/2}$ = 5.7 s), which completely decays to its ground state by an IT (100%) process. Therefore the measured cross-sections of ^{103g}Ag are cumulative. The radionuclide ^{103g}Ag was identified by its independent γ-lines of 118.74 keV (31.2%) and 148.2 keV (28.3%), and consistent results was found between them. The ^{103}Ag production cross-section (Fig. 5) starting from its experimental threshold around 15 MeV (far from its theoretical one of 12.87 MeV) increased gradually up to a maximum value about 537 mb at 26.3 MeV.

As depicted in Fig. 5, the measured energy range is not enough to identify the peak of the excitation function of $^{103g+m}$Ag. However, EMPIRE calculation indicates that the peak position is at 27 MeV. EMPIRE calculation matches the experimental cross section, within the acknowledged error, in the 17-22 MeV energy range, and then it underestimates the measured values at higher energies. Therefore, it is not a trustworthy calculation to speculate the peak position or shape of the excitation function. TENDL data has much lower magnitude and down position at the energy scale.

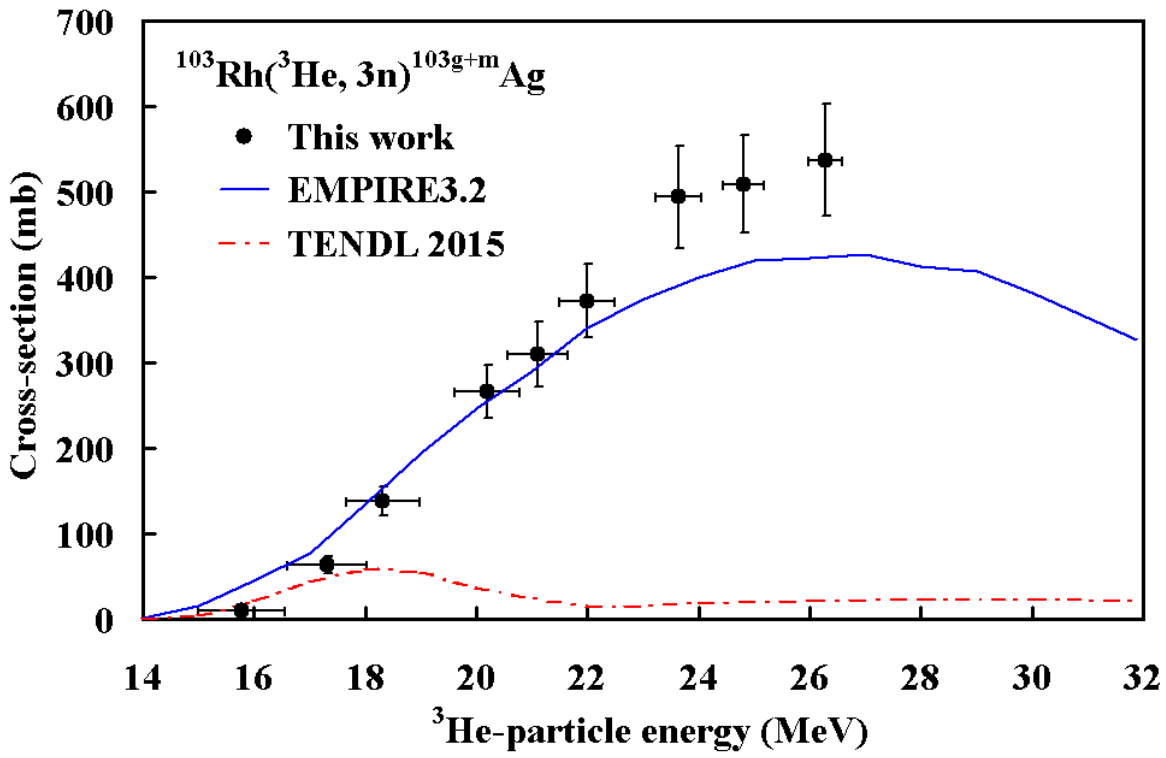

Fig 5: Excitation function of the ^{103}Rh(^{3}He,3n)$^{103g+m}$Ag reaction.

Excitation function for the ^{103}Rh(^{3}He, *x*) $^{100, 101m, 101, 102m, 102g}$Rh reactions

For the ^{102}Rh observed, the very low isomeric transition ratio (0.23%) of ^{102m}Rh , which is much less than the experimental error (11-13%), and the long half-life of the ^{102m}Rh (see Table 1) allow for considering that shortly after EOB the nuclei in the ground state originate only from direct formation. The excitation functions for both isomers separately are given in Figs. 5 and 6 in comparison with the theoretical results.

In both cases, the experimental excitation function exhibits a progressively increasing behavior with increasing energy, starting from the experimental threshold till the end of measurement range of 26.3 MeV. In contrast, the theoretical calculations reflect a complex behavior, demonstrating a low energy broad peak around 16 MeV in case of ^{102m}Rh and around 18 MeV in case of ^{102g}Rh. TENDL data has a flat top of that peaks. Then, both TENDL and EMPIRE data have a progressively increasing cross sections with increasing energy. EMPIRE calculations relies only on the ^{103}Rh(^{3}He, α) (100%) process. Whereas TENDL appends to the (^{3}He, α) (100-20%) process a contribution of (^{3}He, p t) (3-35%) and (^{3}He, n ^{3}He) (3-45%) processes at energies above 20 MeV up to the presented range of 30 MeV. Beyond 30 MeV, TENDL appends a contribution of (^{3}He, n p d) and (^{3}He, 2n 2p) processes.

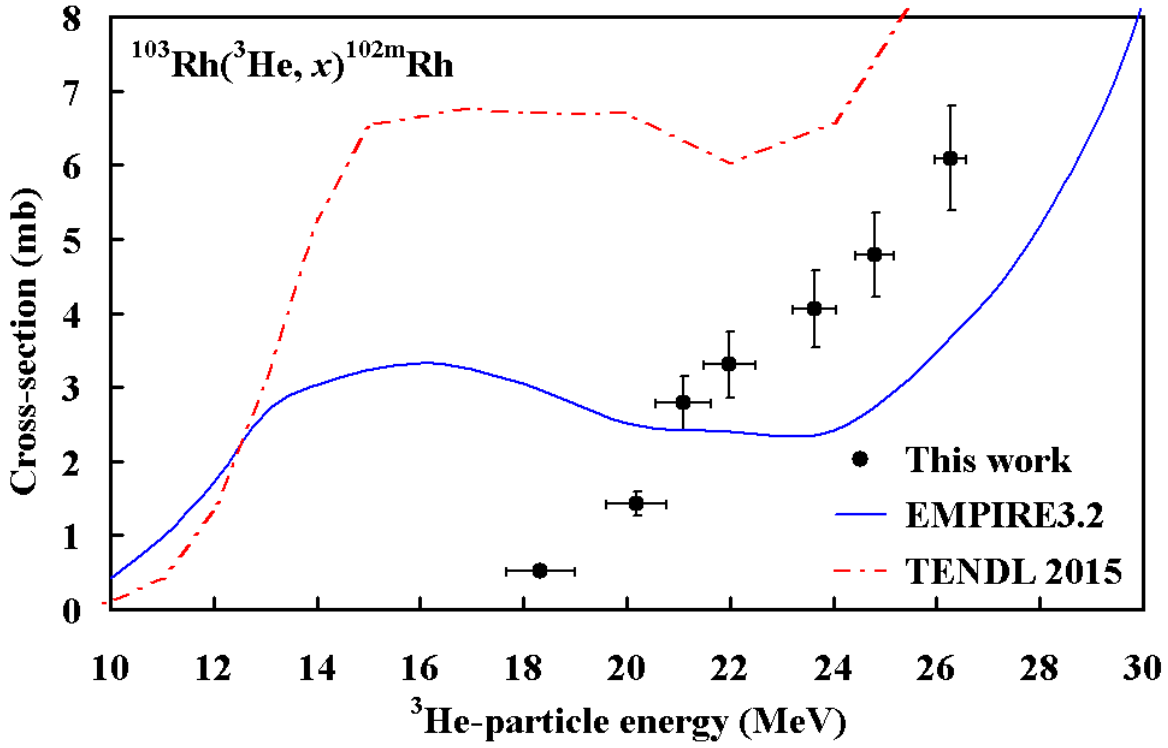

Fig 6: Excitation function of the ^{103}Rh(^{3}He, *x*)^{102m}Rh reaction.

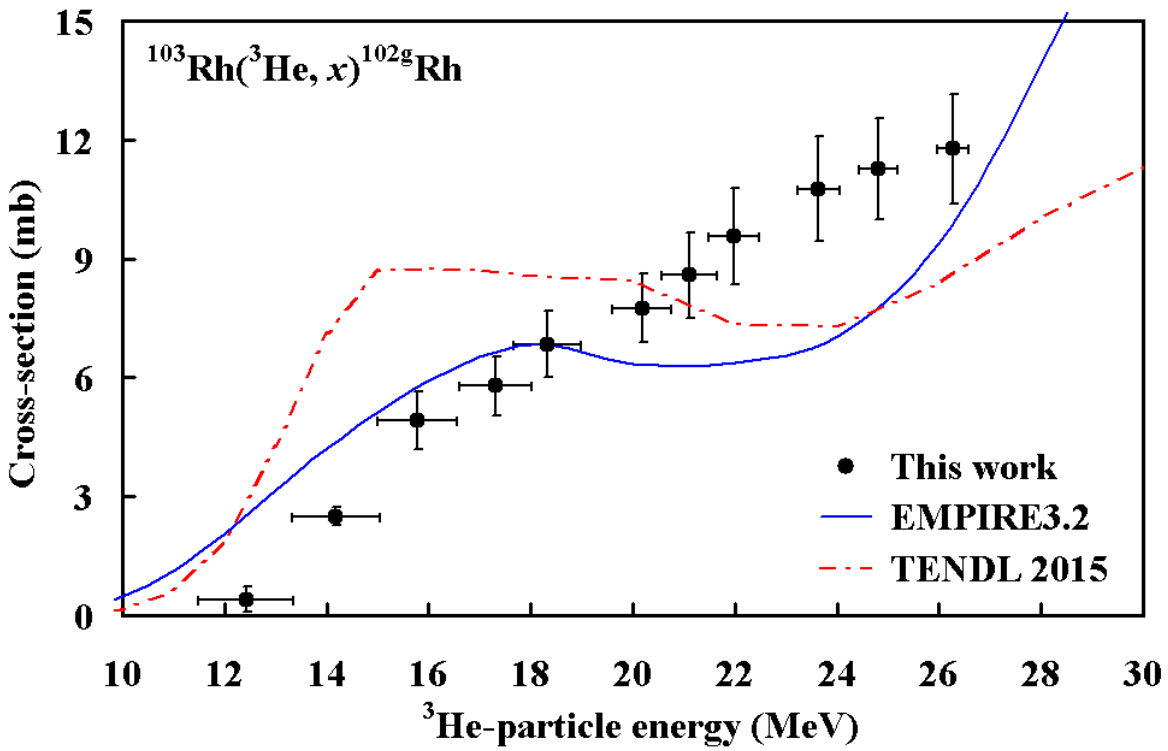

Fig 7: Excitation function of the ^{103}Rh(^{3}He, x)^{102g}Rh reaction.

The excited isomeric state, ^{101m}Rh, with a half-life of 4.34 d, decays for 7.20% by isomeric transition to the long-lived ($T_{1/2}$ = 3.3 y) ground state ^{101g}Rh. The different and independent γ-lines emitted during the decay of excited and ground states allow determining the activity of both isomers at different times after end of irradiation. The respective excitation functions are shown in Figs. 8 and 9 in comparison with the theoretical results.

Both measured excitation functions exhibit a noticeable peak around about 23 MeV and have the same order of magnitude. TENDL data can not reproduce any of the experimental excitation function main features; neither shape, magnitude nor peak position. EMPIRE calculated excitation function has nearly the same shape as the experimental ones with peak position slightly down shifted to 22 MeV. EMPIRE overestimates the calculated cross sections to various extend.

TENDL and EMPIRE account the calculated cross section to the (^{3}He, n α) process in the studied energy range. Thereafter, TENDL involves other reaction channels; as (^{3}He, n p t) starting from 28 MeV, (^{3}He, n ^{3}He) starting from 30 MeV, etc.

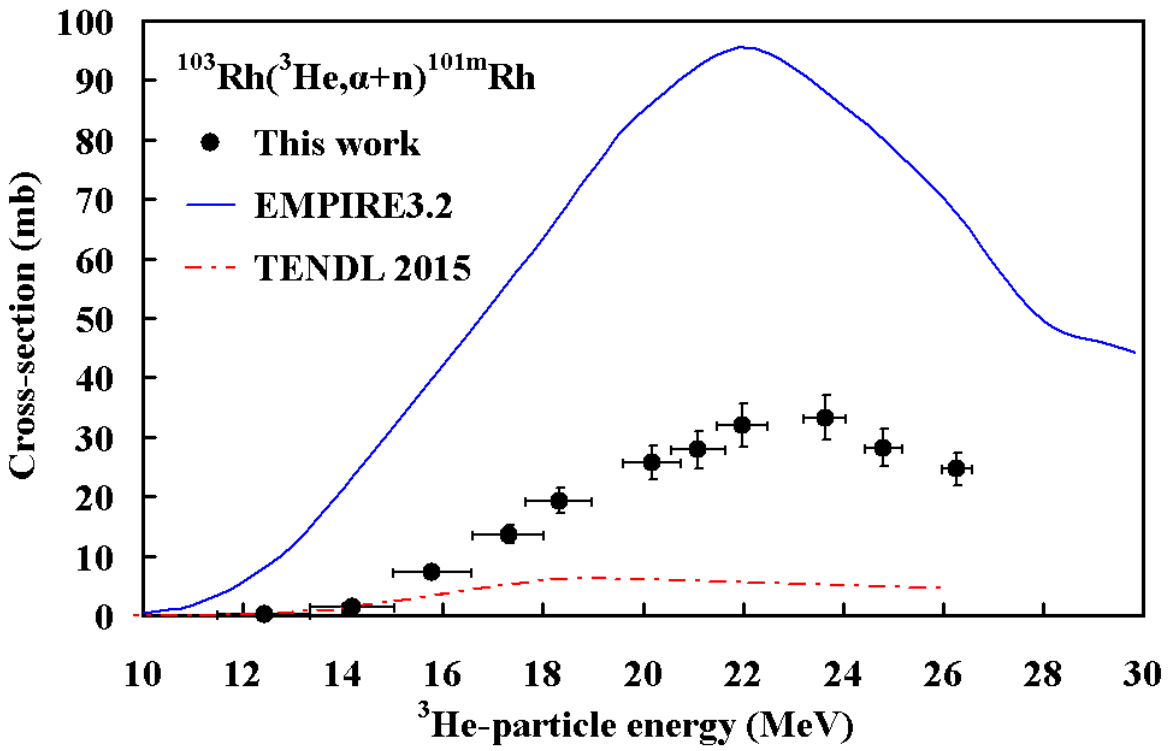

Fig 8: Excitation function of the ^{103}Rh(^{3}He,α+n)^{101m}Rh reaction.

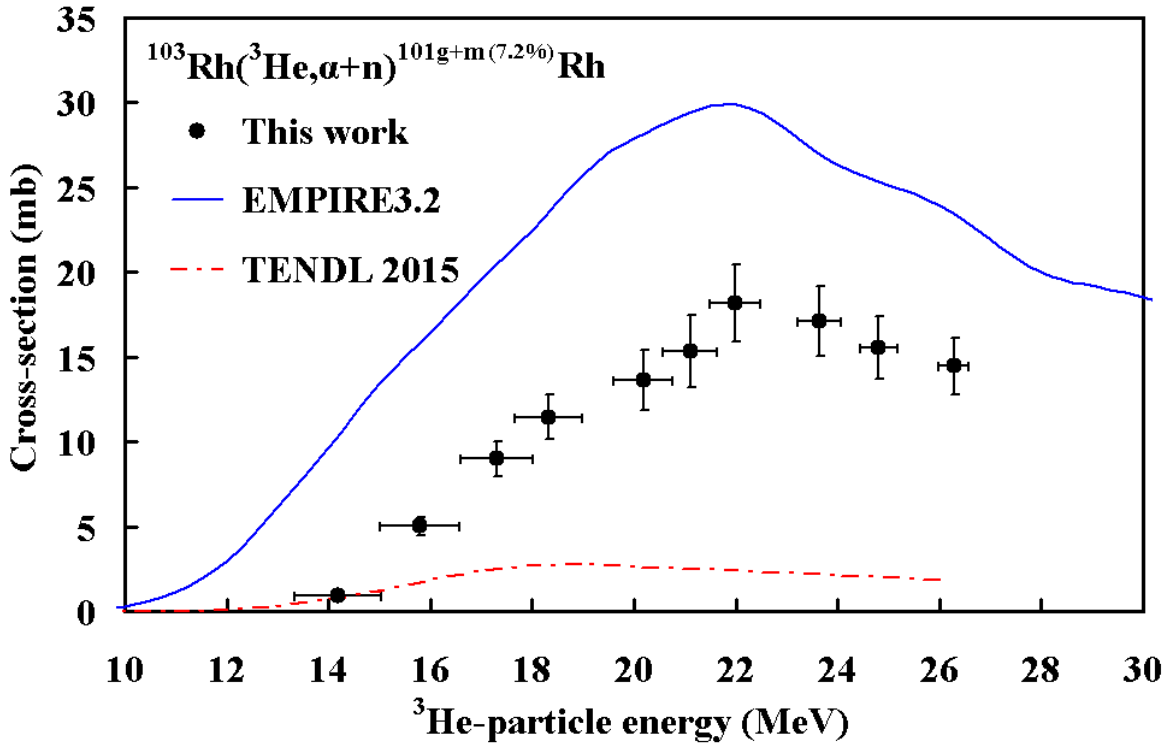

Fig 9: Excitation function of the ^{103}Rh(^{3}He,α+n)$^{101g+m}$Rh reaction.

The residual nucleus ^{100}Rh, produced through the ^{103}Rh(^{3}He, α+2n)^{100}Rh reaction, has two isomers ^{100m}Rh ($T_{1/2}$ = 4.7 min) and ^{100g}Rh ($T_{1/2}$ = 20.8 h). The decay of metastable state to the ground state is mostly through isomeric transition (98.3%) and the remaining through electron capture along with β^+ decay. In this case the total cross-section was measured by allowing for complete decay of metastable state to the ground state (see Fig. 10).

The excitation function shows steady increase in the measurement energy rage. The experimental data agree with the theoretical ones in the general shape. However, each data set has its own increasing rate, reflecting EMPIRE overestimation and TENDL underestimation behavior.

In spite of the cross section overestimation of the EMPIRE calculation, it owns all the cross section to the ground state with zero participation of the metastable state. On the contrary, TENDL underestimates the calculated cross sections, but it gives an appreciable weight to the metastable contribution (49-63%) regarding the cumulative cross section. Both codes attribute the calculated excitation function to the (^{3}He,2nα) reaction channel in the studied energy range, and TENDL starts to include other channels starting from about 40 MeV.

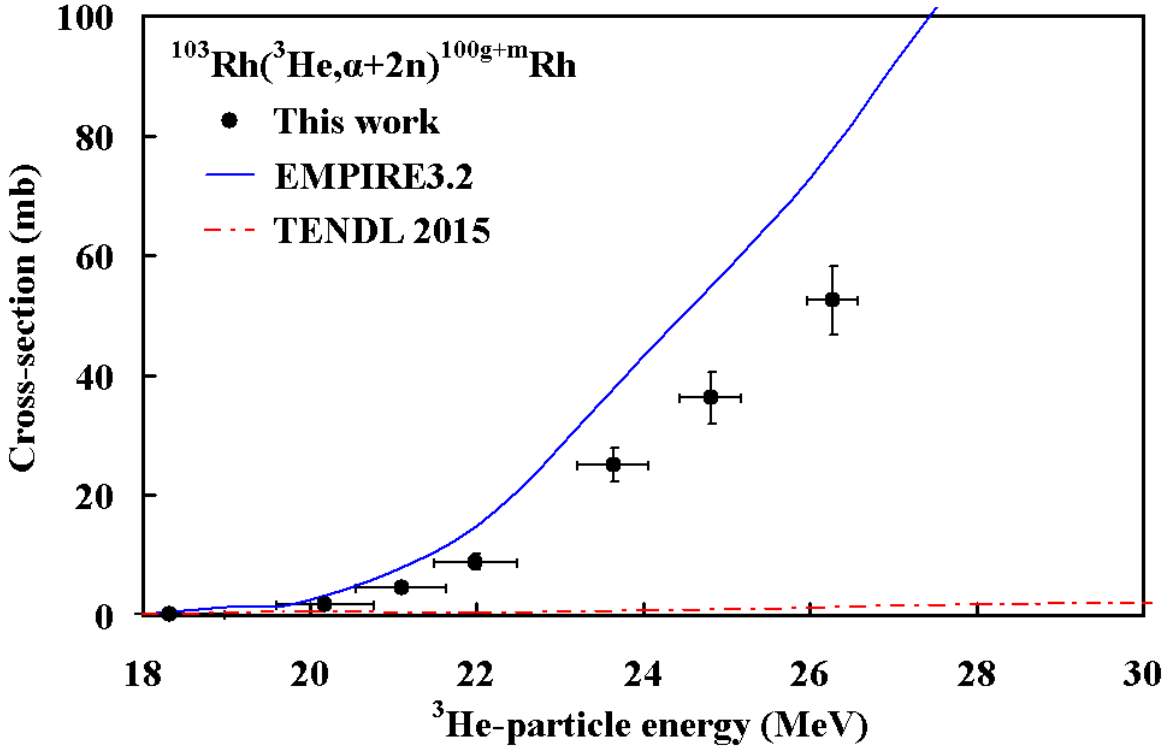

Fig 10: Excitation function of the ^{103}Rh(^{3}He,α+2n)$^{100g+m}$Rh reaction.

Excitation function for the ^{103}Rh(^{3}He, x) ^{103cum}Pd reaction

The most straightforward way to assess the activity of ^{103}Pd seems to be direct measurement of the strong, not resolved, X-ray complexes of the de-excitation of the ^{103}Rh daughter nuclei (K_{a1}+K_{a2}: 64.7%; K_{b1}+K_{b2}: 12.34%). These lines can however be contaminated with spurious signals coming from different origins [1]. The work has been performed by Ditrói et al. [4] considered only the weak 357 keV gamma-ray detection that showed enough counts from ^{103}Pd decay. It should be mentioned that there are discrepancies in ^{103}Pd assessment [1]. A difference up to 25% between activities determined by means of X- and gamma-lines was found if the adopted absolute intensities of the X-rays and the 357 keV gamma-ray, available at the moment of publication were used. For preparation of the IAEA recommended data file [18] the experimental data obtained via the X-ray measurements were used, but the decay data measurements [19] confirm the earlier use of absolute intensities of the weak gamma line. In the present work the gamma-line of 357 keV detection was used.

In addition to the production of ^{103}Pd by the ^{103}Rh(^{3}He, *x*) reactions it is also formed by indirect route; through ^{103}Ag/^{103}Pd generator. The indirect route has been optimistically suggested for production of ^{103}Pd [19-21]. Fig. 5 and 11 reveals that both reaction routes have appreciable cross section, which supports the ^{103}Rh(^{3}He, *x*) as a future means for production of ^{103}Pd. As in case of ^{103}Ag, without any significant difference, the measured energy range can't disclose any information about the shape or extend of the excitation function peak. Nevertheless, EMPIRE calculation indicates that the peak position is around 30 MeV (Fig. 10). EMPIRE calculation matches the experimental cross section, within the acknowledged error, in a very limited energy range of 15-18 MeV, and then it underestimates the measured values at higher energies. TENDL data result in an odd excitation function, which can not describe the experimental one. EMPIRE calculation attributes the ^{103}Rh(^{3}He, *x*) ^{103}Pd reaction to the (^{3}He, t) (100%) process, meanwhile TENDL ascribe it to the (^{3}He, t) (100-84%) , (^{3}He, n d) (2-6%) , (^{3}He, t) (1-10%) processes. EMPIRE calculation reveals that the $^{103g+m}$Ag decay subscribe with up to 50% to the cumulative cross section, while TENDL data gives it less than 5% share, in the scope of studied energy range.

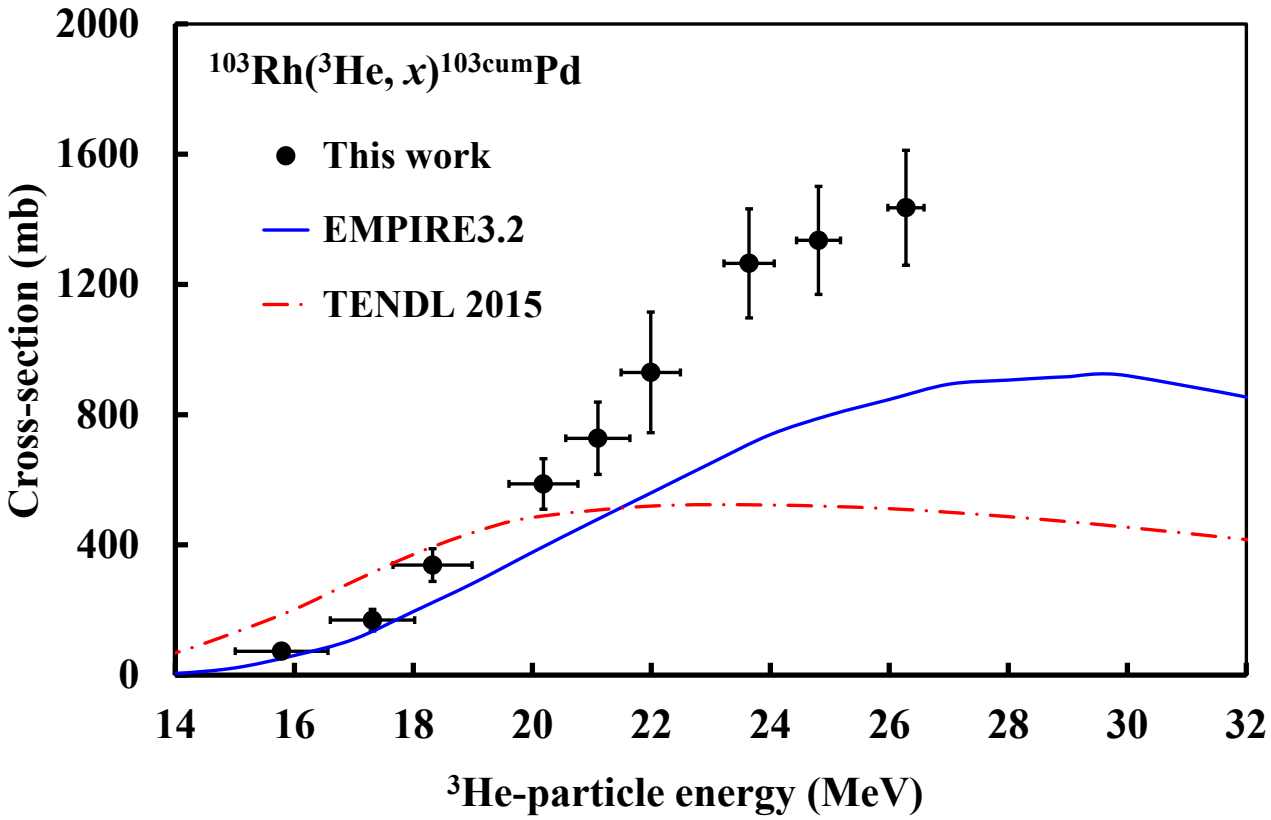

Fig 11: Excitation function of the ^{103}Rh(^{3}He,x)^{103}Pd reactions.

Integral yields

The cyclotron production of a medical radionuclide demands consideration of cross-section data not only of the desired reaction but also of other competing reactions leading to possible disturbing radioactive impurities, such as $^{100,\ 101,\ 101m,\ 102m,\ 102}$Rh and $^{103,\ 104m,\ 104,\ 105}$Ag along with ^{103}Pd. Prior knowledge of their activities facilitates the following chemical treatment of irradiated target, and estimating the hazards associated with utilization required useful radionuclide. Consequently, in this section the integral yield at incident ^{3}He energy of 27 MeV, will be calculated for all possibly produced radionuclides.

The integral yields (Fig. 12) were calculated on the basis of the experimental excitation functions shown in Figs. 2–11. For the most important radionuclide, ^{103}Pd, its yield was 550 kBq/μAh. For radio-rhodium isotopes of $^{100,\ 101m}$Rh their yields at 27 MeV were significant values of 260 and 55 kBq/μAh, respectively, while the other radio-rhodium isotopes produced show negligible yield values. On the other hand the yields at 27 MeV of all radio-silver isotopes produced were appreciable values of 57, 17, 22 MBq/μA.h for $^{103,\ 104m,\ 104g}$Ag, respectively, except the yield of ^{105}Ag, which was also a negligible value.

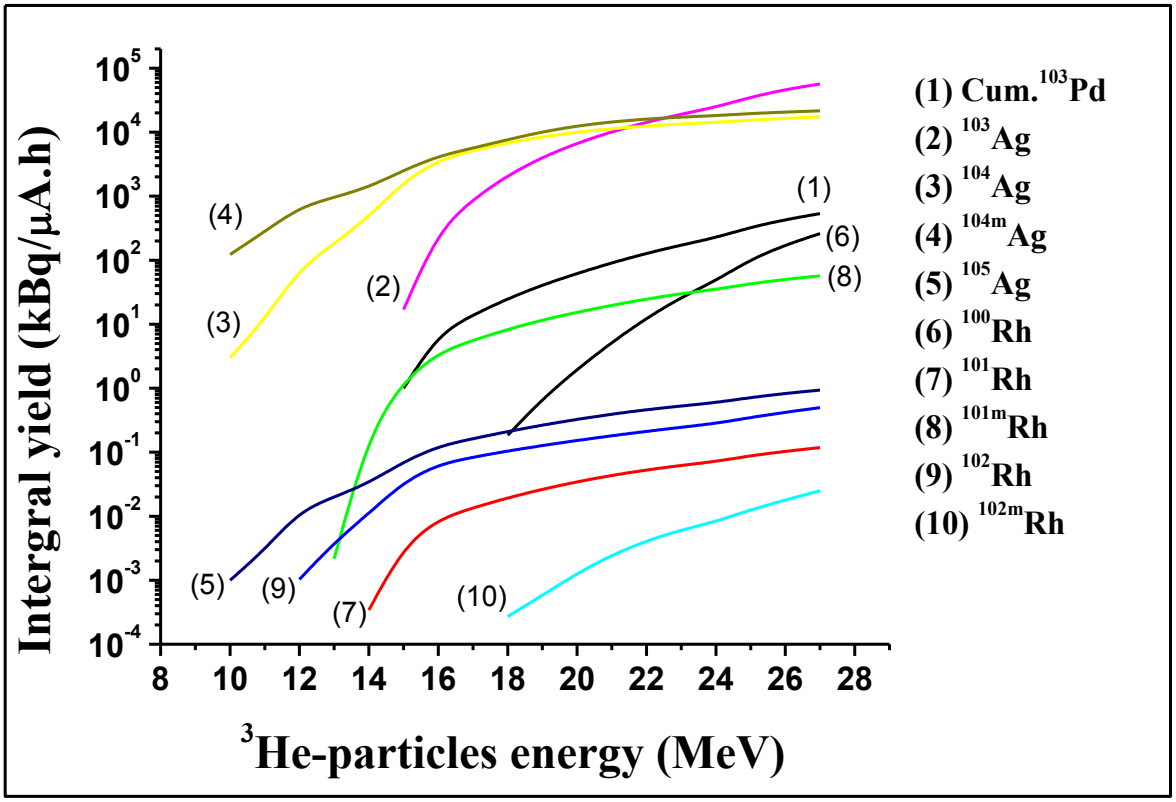

Fig 12: Integral yields for the formation of ^{103,104,105}Ag, ^{103}Pd and ^{100,101,102}Rh radionuclides through different ^{103}Rh (^{3}He, x) reaction channels.

Conclusion

Searching of data in the literature for particle induced reactions, only proton, deuteron and α-particle induced reactions on rhodium were found. Meanwhile, there were no available data for ^{3}He-particle induced reactions on rhodium that is the aim of this work. ^{103}Pd and $^{100,\ 101m,\ 101,\ 102m,}$ ^{102}Rh were formed through the different reactions in ^{3}He-activation of ^{103}Rh not as of $^{103,\ 104,\ 105}$Ag. The production of radionuclides of Ag includes the following; the measured excitation function of ^{105}Ag reached its maximum value around 23.6 MeV. For ^{104}Ag there are two independent isomeric states, ^{104m}Ag and ^{104g}Ag. Their excitation functions have defined peaks around about 19 and 17.5 MeV, respectively. For ^{103}Ag there was defined peak of excitation function. In the production of radionuclides of Rh the excitation functions had defined peaks for $^{101m,\ 101}$Rh, while for $^{100,\ 102m,}$ ^{102}Rh the peaks haven't identified. Also, the excitation function of ^{103}P had no defined peak.

Theoretical calculations of EMPIRE and TENDL succeeded in some cases to describe the experimental excitation function and in some others fail (as mentioned above). The cases explained successfully to some extent were for ^{103}Pd, $^{100,\ 102}$Rh and ^{103}Ag.

The integral yield of the all radionuclides produced was calculated. The yield of the most important medical radionuclide, ^{103}Pd, was an appreciable value of 550 kBq/μAh but rather low with that obtained by proton and deuteron activations of ^{103}Rh. By consideration of the radionuclide impurities in proton and deuteron activation the ^{3}He-activation of ^{103}Rh could be taken an alternative pathway for the production of it.

References

1. Hermanne, A., Sonck, M., Fenyvesi, A., Daraban, L., 2000. Study on production of ^{103}Pd and characterization of possible contaminants in the proton irradiation of ^{103}Rh up to 28 MeV. Nucl.Instrum.MethodsPhys.Res.B170, 281–292.
2. Sudár,S., Cserpák, F., Qaim,S.M., 2002.Measurements and nuclear model calculations on proton-induced reactions on 103Rh up to 40MeV:evaluation of the excitation function of the ^{103}Rh(p,n)^{103}Pd reaction relevant to the production of the therapeutic radionuclide ^{103}Pd. Applied Radiation and Isotopes 56, 821–831.
3. A. Hermanne, M. Sonck, S. Takács, F. Tárkányi, Y. Shubin, Nucl. Instrum. Meth. B 187 (2002) 3.
4. F. Ditrói, F. Tárkányi, S. Takács, A. Hermanne, H. Yamazaki, M. Baba, A. Mohammadi, A.V. Ignatyuk. "Study of activation cross-sections of deuteron induced reactions on rhodium up to 40 MeV" Nuclear Instruments and Methods in Physics Research B 269 (2011) 1963–1972
5. G. W. A. Newton, V. J. Robinson and E. M. Shaw "^{103}Rh(a, xn) $^{107-X}$Ag reactions" J. inorg, nucl. Chem. Vol. 43. No. 10. pp. 2227-2232, 1981.
6. M. S. Gadkari and N. L. Singh "α-Particle induced reactions on rhodium" Pramana journal of physics 62, 1059-1072 (2004).
7. B. M. Ali, M. Al-Abyad, U. Seddik, S. U. El-Kamessy, F. Ditrói, S. Takács, F. Tárkányi, Experimental investigation and theoretical calculation of ^{3}He-particle induced nuclear reactions on cadmium up to 27 MeV, Nucl. Instr. Meth. Phys. Res. B 321, (2014) 30-40.
8. M. Al-Abyad, F. Tárkányi, F. Ditrói, S. Takács, Excitation function of ^{3}He-particle induced nuclear reactions on natural palladium, App. Radiat. Isot. 94, (2014) 191-199.
9. J. F. Ziegler, M.D. Ziegler, J.P. Biersack, SRIM 2013 code, available from URL http://srim.org.
10. G. Székely, FGM - A Flexible Gamma-spectrum analysis program for a small computer, Comput. Phys. Commun. 34 (3) (1985) 313-324.
11. National Nuclear Data Center, Brookhaven National Laboratory, NuDat 2.6 database, http://www.nndc.bnl.gov/hbin/nudat.
12. F. Tárkányi, S. Takács, K. Gul, A. Hermanne, M.G. Mustafa, M. Nortier, P. Oblozinsky, S.M. Qaim, B. Scholten, Yu.N. Shubin, Z. Youxiang, IAEA TECDOC-1211, Beam monitors

reactions: charged particles cross-sections database for medical radioisotope production, Co-ordinated Research Project, IAEA, Vienna, pp. 77–80, 2001. Available from: http://www.nds.iaea.org/medical (Updated version January 2007).

13. ISO, Guide to Expression of Uncertainty in Measurement, ISBN 92-67-10188- 9. International Organization for Standardization, Geneva (1995).

14. M.U. Khandaker, K.S. Kim, M.-W. Lee, K.-S. Kim, G.N. Kim, Nucl. Instrum. Methods Phys. Res. B 262 (2011) 1140.

15. M.U. Khandaker, M.S. Uddin, K.S. Kim, Y.S. Lee, G.N. Kim, Nucl. Instrum. Methods Phys. Res. B 262 (2007) 171.

16. Z. B. Alfassi, R. Weinreich, The production of positron emitters ^{75}Br and ^{76}Br: Excitation functions and yields for ^{3}He and α-particle induced nuclear reactions on arsenic, Radiochim. Acta 30 (1982) 67-72.

17. M. Fassbender, A. F. Novgorodov, F. Rösch, S. M. Qaim, Excitation functions of ^{93}Nb(^{3}He,*x*n)$^{93m,g,\ 94\ m,g,\ 95m,g}$Tc-processes from threshold up to 35 MeV: Possibility of production of ^{94m}Tc in high radiochemical purity using a thermochromatographic separation technique, Radiochim. Acta 65 (1994) 215-222.

18. F. Tárkányi, M. Nortier, R. Capote, A.V. Ignatyuk, B. Scholten, S.F. Kovalev, B. Király, E. Menapace, Yu.N. Shubin, Charged-particle production of ^{64,67}Cu, ^{67}Ga, ^{86g}Y, ^{102}Rh, ^{103}Pd, ^{111g,114m}In, ^{124,125}I, ^{169g}Yb, ^{177g}Lu, ^{186g}Re, ^{192g}Ir, ^{210,211}At and ^{225}Ac, in: E. Betak et al. (Eds.), Nuclear Data for the Production of Therapeutic Radionuclides, Vienna, IAEA, Technical Reports Series 473 (2011) 143.

19. F. Tárkányi, A. Hermanne, B. Király, S. Takács, F. Ditrói, J. Csikai, A. Fenyvesi, M.S. Uddin, M. Hagiwara, M. Baba, T. Ido, Y.N. Shubin, A.V. Ignatyuk, Appl. Radiat. Isotopes 67 (2009) 1574.

20. Hermanne, A., Takács, S., Tárkányi, F., Bolbos, R., Cross section measurements of proton and deuteron induced formation of ^{103}Ag in natural palladium. Radiochim. Acta 92 (2004) 215–218.

21. Hermanne, A., Tárkányi, F., Takács, S.,Shubin,Yu.N., Experimental determination of cross section of alpha-induced reactions on ^{nat}Pd. Nucl. Instrum. Methods Phys. Res. B 229 (2005) 321–332.

22. F. Szelecsényi, Z. Kovács, K. Nagatsu, M.-R. Zhang, K. Suzuki, Production cross sections of radioisotopes from ^{3}He-particle induced nuclear reactions on natural titanium, Applied Radiation and Isotopes 119 (2017) 94–100.

23. A.J. Koning, D. Rochman, J. Kopecky, J. Ch. Sublet, E. Bauge, S. Hilaire, P. Romain, B. Morillon, H. Duarte, S. van der Marck, S. Pomp, H. Sjostrand, R. Forrest, H. Henriksson, O.

Cabellos, S. Goriely J. Leppanen, H. Leeb, A. Plompen and R. Mills, TALYS-Based Evaluated Nuclear Data Library (Last updated in 5 October 2016). Available from : https://tendl.web.psi.ch/tendl_2015/tendl2015.html .

24. M. Herman, R. Capote, B.V. Carlson, P. Oblozinsky, M. Sin, A. Trkov, H. Wienke, V. Zerkin, EMPIRE: nuclear reaction model code system for data evaluation, Nucl. Data Sheets 108 (12) (2007) 2655–2715.

25. M. Herman et al. , EMPIRE-3.2 (Malta): modular system for nuclear reaction calculations and nuclear data evaluation, User's Manual, Aug. 2013.

Table 1: Decay characteristics of the nuclides studied and Q-values of the contributing reactions.

Radionuclide	$T_{1/2}$	*Some of* E_γ (keV)	I_γ(%)	Contributing reaction	Q-value(MeV)
^{100m}Rh	4.6 min	539.51	1.68	Same reactions of ^{100g}Rh	
		686.97	1.00	except the decay	
^{100g}Rh	20.8 h	446.15	11.98	^{103}Rh(^{3}He, α+2n)	-6.7
		539.5	80.6	^{103}Rh(^{3}He, 2t)	-17.4
		822.7	21.09	^{103}Rh(^{3}He, n+d+t)	-23.7
		1107.2	13.57	^{103}Rh(^{3}He, 2n+p+t)	-25.9
				Decay of ^{100m}Rh by IT: 98.3%	
^{101m}Rh	4.34 d	127.2	0.64	Same reactions of ^{101g}Rh	
		306.9	8.1	except the decay	
		545.1	4.3		
^{101g}Rh	3.3 y	127.2	68	^{103}Rh(^{3}He, α+n)	3.82
		198.0	73	^{103}Rh(^{3}He, d+t)	-13.76
		325.2	11.8	^{103}Rh(^{3}He, n+p+t)	-15.99
				^{103}Rh(^{3}He,2n+^{3}He)	-16.76
				^{103}Rh(^{3}He, n+2d)	-20.02
				^{103}Rh(^{3}He, 2n+p+d)	-22.25
				^{103}Rh(^{3}He, 3n+2p)	-24.47
				Decay of ^{101m}Rh by IT: 7.2%	
^{102m}Rh	3.74 y	418.52	9.4	Same reactions of ^{102g}Rh	
		575.06	95	except the decay	
		631.29	56		
		697.48	44		
		766.84	34		
^{102g}Rh	207.3 d	468.58	2.9	^{103}Rh(^{3}He, α)	11.3
		475.06	4.6	^{103}Rh(^{3}He, p+t)	-8.6
		1103.16	4.5	^{103}Rh(^{3}He, n+^{3}He)	-9.3
				^{103}Rh(^{3}He, 2d)	-12.6
				^{103}Rh(^{3}He, n+p+d)	-14.8
				^{103}Rh(^{3}He, 2n+2p)	-17.0
				Decay of ^{102m}Rh by IT: 0.23%	
^{103}Pd	16.99 d	357.45	0.0221	^{103}Rh(^{3}He, t)	-0.56
				^{103}Rh(^{3}He, n+d)	-6.82
				^{103}Rh(^{3}He, p+2n)	-9.04
				Decay of ^{103}Ag by β^+: 100%	
^{103m}Ag	5.7 s	134.44	4.5	^{103}Rh(^{3}He, 3n)	
^{103g}Ag	65.7 min	118.7	31.2	^{103}Rh(^{3}He, 3n)	-12.51
		148.2	28.3	Decay of ^{103m}Ag by IT: 100%	
		243.9	8.5		
		266.9	13.3		
		1273.8	9.4		
^{104m}Ag	33.5 min	555.8	90	^{103}Rh(^{3}He, 2n)	
		785.7	1.9		
		1238.8	3.9		
^{104g}Ag	69.2 min	555.8	92.6	^{103}Rh(^{3}He, 2n)	-4.12
		740.5	7.2	Decay of ^{104m}Ag by IT: 0.07%	
		758.7	6.4		
		767.6	65.7		
		785.7	9.5		
		857.9	10.4		
		925.9	12.5		
		941.6	25		
		1341.8	7.3		
^{105m}Ag	7. 23 min	319.14	0.163	^{103}Rh(^{3}He, n)	
^{105g}Ag	41.29 d	280.4	30.2	^{103}Rh(^{3}He, n)	5.91
		319.2	4.4	Decay of ^{105m}Ag by IT: 100%	
		344.5	41.4		

	644.6	11.1
	1087.9	3.9

Table 2: Cross-sections for the formation of $^{103g+m}$Ag, ^{104m}Ag, ^{104g}Ag, and $^{105g+m}$Ag radionuclides

E_{3He} (MeV)	$^{105g+m}$Ag	^{104m}Ag	^{104g}Ag	$^{103g+m}$Ag
	σ(mb)	σ(mb)	σ(mb)	σ(mb)
26.28	3.7 ± 0.4	28 ± 3	49.8 ± 12.3	537 ± 65
24.81	3.8 ± 0.4	32 ± 4	62.2 ± 8.3	509 ± 57
23.64	4.3 ± 0.5	63 ± 7	87.3 ± 13.6	494 ± 60
21.99	4.1 ± 0.5	82 ± 9	106.6 ± 13.6	372 ± 43
21.10	3.9 ± 0.5	106 ± 12	119.4 ± 16.7	309 ± 38
20.19	3.9 ± 0.5	144 ± 16	135.8 ± 20.1	266 ± 31
18.32	3.2 ± 0.4	141 ± 16	153.7 ± 17.8	138 ± 17
17.31	2.5 ± 0.3	108 ± 12	157.2 ± 21.3	63 ± 10
15.78	1.3 ± 0.1	66 ± 7	102.7 ± 11.6	10 ± 1
14.19	1.0 ± 0.1	27 ± 3	29.6 ± 3.4	
12.42	0.4 ± 0.1	3 ± 0.2	5.2 ± 0.6	

Table 3: Cross-sections for the formation of $^{100g+m}$Rh, ^{101m}Rh, $^{101g+m}$Rh , ^{102m}Rh and ^{102g}Rh radionuclides

E_{3He} (MeV)	$^{100g+m}$Rh	^{101m}Rh	$^{101g+m}$Rh	^{102m}Rh	^{102g}Rh
	σ(mb)	σ(mb)	σ(mb)	σ(mb)	σ(mb)
26.28	52.5 ± 5.8	24.6 ± 2.8	14.5 ± 1.7	6.1 ± 0.7	11.8 ± 1.4
24.81	36.3 ± 4.3	28.2 ± 3.2	15.5 ± 1.9	4.8 ± 0.6	11.3 ± 1.3
23.64	25.1 ± 2.8	33.3 ± 3.7	17.1 ± 2.1	4.1 ± 0.5	10.8 ± 1.3
21.99	8.9 ± 1.2	32.0 ± 3.6	18.2 ± 2.3	3.3 ± 0.4	9.6 ± 1.2
21.10	4.6 ± 0.5	27.9 ± 3.1	15.3 ± 2.1	2.8 ± 0.4	8.6 ± 1.1
20.19	1.8 ± 0.2	25.7 ± 2.9	13.6 ± 1.8	1.4 ± 0.2	7.8 ± 0.9
18.32	0.2 ± 0.1	19.3 ± 2.2	11.5 ± 1.3	0.5 ± 0.1	6.8 ± 0.8
17.31		13.7 ± 1.5	9.0 ± 1.0		5.8 ± 0.7
15.78		7.2 ± 0.8	5.0 ± 0.5		4.9 ± 0.7
14.19		1.4 ± 0.2	0.9 ± 0.2		2.5 ± 0.2
12.42		0.3 ± 0.1			0.4 ± 0.3

Table 4: Cross-sections for the formation of ^{103}Pd radionuclide

E_{3He} (MeV)	σ(mb)
26.28	1435.6 ± 176.5
24.81	1335.4 ± 166.1
23.64	1264.7 ± 167.7
21.99	929.7 ± 185.2
21.10	727.5 ± 111.3
20.19	587.4 ± 77.7
18.32	338.0 ± 50.4
17.31	169.0 ± 33.3
15.78	73.5 ± 20.1